First-principle calculations of electron, phonon, optic and thermodynamic properties of CdSe and CdS crystals

A. I. KASHUBA[1,*], I. V. SEMKIV[1], H. A. ILCHUK[1], R. Y. PETRUS[1], V. M. KORDAN[2], S. V. SHYSHKOVSKYI[1]
[1]*Lviv Polytechnic National University, Bandera Str. 12, 79646 Lviv, Ukraine*
[2]*Ivan Franko National University of Lviv, Kyrylo & Mephodiy Str. 6, 79005 Lviv, Ukraine*

Electronic and phonon band structure, thermodynamic and optical properties are studied for the CdSe and CdS crystals. We calculated the electron and phonon dispersion at high symmetry directions, density of electron and phonon state, temperature dependence feature of Raman spectra, heat capacity, free energy, entropy, enthalpy and Debye temperature estimated with the generalized gradient approximation (GGA). A Perdew–Burke–Ernzerhof functional (PBEsol) was utilized. To study the optical properties was use a complex dielectric function ε(ħω). All of the calculated parameters correlate well with the known experimental data.

(Received August 16, 2021; accepted October 5, 2022)

Keywords: Density functional theory, Band structure, Optical functions, Thermodynamic properties

1. Introduction

Semiconductor compounds $A^{II}B^{VI}$ have many important applications in solar cell, efficient thin film transistors and light-emitting diodes [1, 2]. In spite of extensive experimental and theoretical studies of these materials, some of their fundamental parameters are still unknown. On the other hand, this information is very important for modeling and developing different optical and electronic devices. Some portion of information on the physical properties of CdSe and CdS crystals has been presented in the previous literature [3, 4]. Most of them have been focused on the optical and electrical parameters.

Among numerous theoretical studies of the electronic and phonon band structure [1–4], the optical parameters [3, 4] of CdSe and CdS compounds, we have not found the full results for the temperature behavior of basic thermodynamics parameters (Debye temperature) and Raman spectra.

In this work, we report on the fundamental electron and phonon properties of the CdSe and CdS crystals. Having performed the electronic band-structure calculations for CdSe and CdS, one can obtain their optical parameters. Finally, we have derived the temperature dependence of Raman spectra, free energy, heat capacity, entropy, enthalpy and Debye temperature.

2. Methods of calculation

The theoretical calculations were performed within the framework of the density functional theory (DFT). To calculate the properties of single-crystalline CdS and CdSe, a crystalline lattice with the basal parameters given below was used. The Vanderbilt's ultrasoft pseudopotentials [5] were used for the ion potentials. To describe the exchange-correlation energy of the electronic subsystem, a functional in the approximation of generalized gradient (GGA) and the Purdue–Burke–Ernzerhof (PBEsol) parameterization [6] was used. As a correlation potential, the Ceperlay–Alder and Gell–Mann–Brueckner equations were applied to the high electron-density boundaries.

The charge-density distribution was calculated by the method of special points involving the techniques of charge damping. The relaxation of ion positions on the basis of calculated atomic forces was achieved for each crystal structure, and then the integral stress of the cell was determined.

The value $E_{\text{cut-off}}$= 660 eV for the energy of cutting-off the plane waves was used in our calculations. The electron configurations $4d^{10}5s^2$ for Cd, $3s^23p^4$ for S and $4s^24p^4$ for Se atoms formed the valence electron states. The integration over the Brillouin zone (BZ) was performed on the 4×4×2 grid of k points using the Monkhorsta–Pack scheme [7]. The self-consistent convergence of the total energy was taken as 5.0×10^{-6} eV/atom. For DFT calculations of CdSe and CdS crystals the 3×3×3 supercell containing 256 atoms has been created. The hexagonal structure ($P6_3mc$) has been used for the optimized structure of the crystal supercell $Cd_{16}Se_{16}$ ($Cd_{16}S_{16}$). Geometry optimization of the lattice parameters and atomic coordinates were performed using the Broyden–Fletcher–Goldfarb– Shanno (BFGS) minimization technique with the maximum ionic Hellmann–Feynman forces within 0.01 eV/Å, the maximum ionic displacement within 5.0×10^{-4} Å, and the maximum stress within 0.02 GPa. These parameters are sufficiently small to lead to a well-converged total energy of the structures studied.

The energy band diagram was constructed using the points of the BZ in the inverse space, which were as follows: G(0, 0, 0), A(0, 0, 0.5), H(–0.333, 0.667, 0.5), K(–0.333, 0.667, 0), M(0, 0.5, 0) and L(0, 0.5, 0.5).

3. Results and discussion

3.1. Electron band energy structure

In Fig. 1, the full energy band diagrams of the CdS and CdSe crystals are shown along the highly symmetric lines of the tetragonal BZ. The energy in this case is counted from the Fermi level. Analysis of the results of theoretical calculations of the energy band spectrum shows that the smallest bandgap is localized in the center of the BZ (the point G). This means that the crystal is characterized by a direct energy bandgap. Our bandgaps E_g prove to be less than the appropriate parameters derived experimentally for both pure CdSe (~1.71 eV [8]) and CdS (~2.47 eV [9]). Note, however, that the generalized gradient approximation always suffers from unavoidable underestimation of the bandgap (see Table 1).

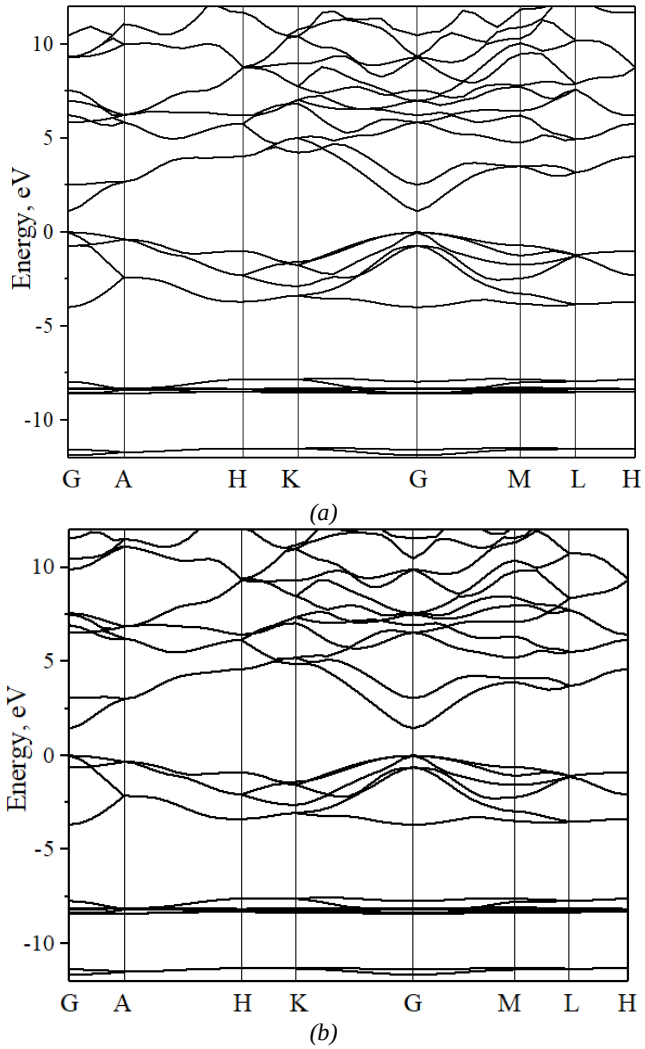

Fig. 1. Electron band energy structure of CdSe (a) and CdS (b) crystals

Table 1. Parameters of calculated for CdSe and CdS crystals (for hexagonal structure ($P6_3mc$))

Parameters	Material	Calculation value	Experimental value
$a = b$, Å	CdSe	4.370813	4.277(5) [10]
c, Å		7.076424	6.981(8) [10]
E_g, eV		1.128	~1.71 [8]
$a = b$, Å	CdS	4.265490	4.048(16) [3]
c, Å		6.894737	6.66(4) [3]
E_g, eV		1.449	~2.47 [9]

The underestimation of the bandgap is a known issue with this calculation approach. The easiest way to get the results closer to experimental ones is to use a so-called 'scissor' operator, which leads to changing the bandgap by shifting the conduction band into the region of higher energies. This operator is based on the proximity of the $E(k)$ dispersion dependences of the energies of conduction bands, which are determined from the Kohn–Sham equations [11]. The conduction bands of the calculated energy spectrum are usually shifted until the experimental value of the minimum energy gap bandwidth E_g of the crystal is achieved. In this work, the calculated value was corrected to the value of $\Delta E = 0.582$ eV for CdSe and $\Delta E = 1.021$ eV for CdS to bring the absolute E_g values into agreement. However, this does not affect the overall trend in the electronic and structural properties, which is

confirmed by a number of previous calculations of the electronic states [12, 13].

The analysis of partial contributions of individual levels to the function of the total density of states (Fig. 2) and the partial contributions of individual bands to the electronic density allows us to find genesis of the valence and conduction bands for the CdSe and CdS crystals. The lowest bands from –12 to –10 eV are formed by the *s* states of Se (S). The following bands dispersed at the energy marker from –9 to –6 eV are formed because of the contributions of the *d* states of Cd. The peak of the valence complex is practically formed by the *p* states of Se (S), with 'contamination' of the *p* states of Cd. But the conduction band bottom is mainly formed by the *p* states of Cd and Se (S), as well as by the *s* states of Cd.

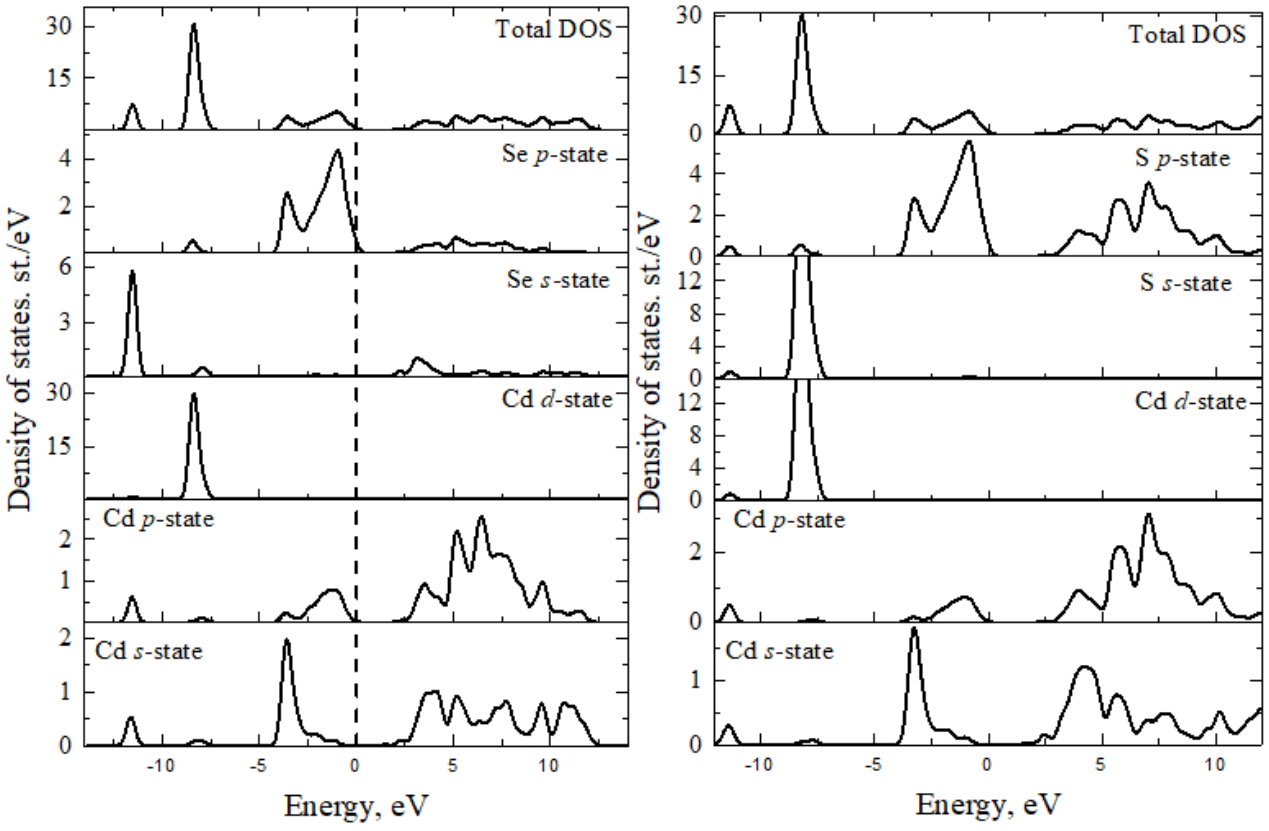

(a) *(b)*

Fig. 2. Electron density of states of CdSe (a) and CdS; (b) crystals

3.2. Phonon band energy structure

The curves of phonon dispersion ω_p and total phonon density of states of CdSe and CdS at several high symmetry BZ points are represented in Fig. 3. As it has been known [3, 10], a crystal lattice consisting of four atoms per unit cell has 12(3×4) branches in which three of them are acoustic and the rest are optical. It can be seen that 3 acoustic branches that correspond to sound propagation as $q \to 0$ and 9 optical branches emerge from point G (with $\omega = 0$). The acoustic modes are including the longitudinal acoustic (LA) and transverse acoustic (TA) modes. The highest phonon frequency of ~6.17 THz and ~8.54 THz was found at point G for CdSe and CdS, respectively.

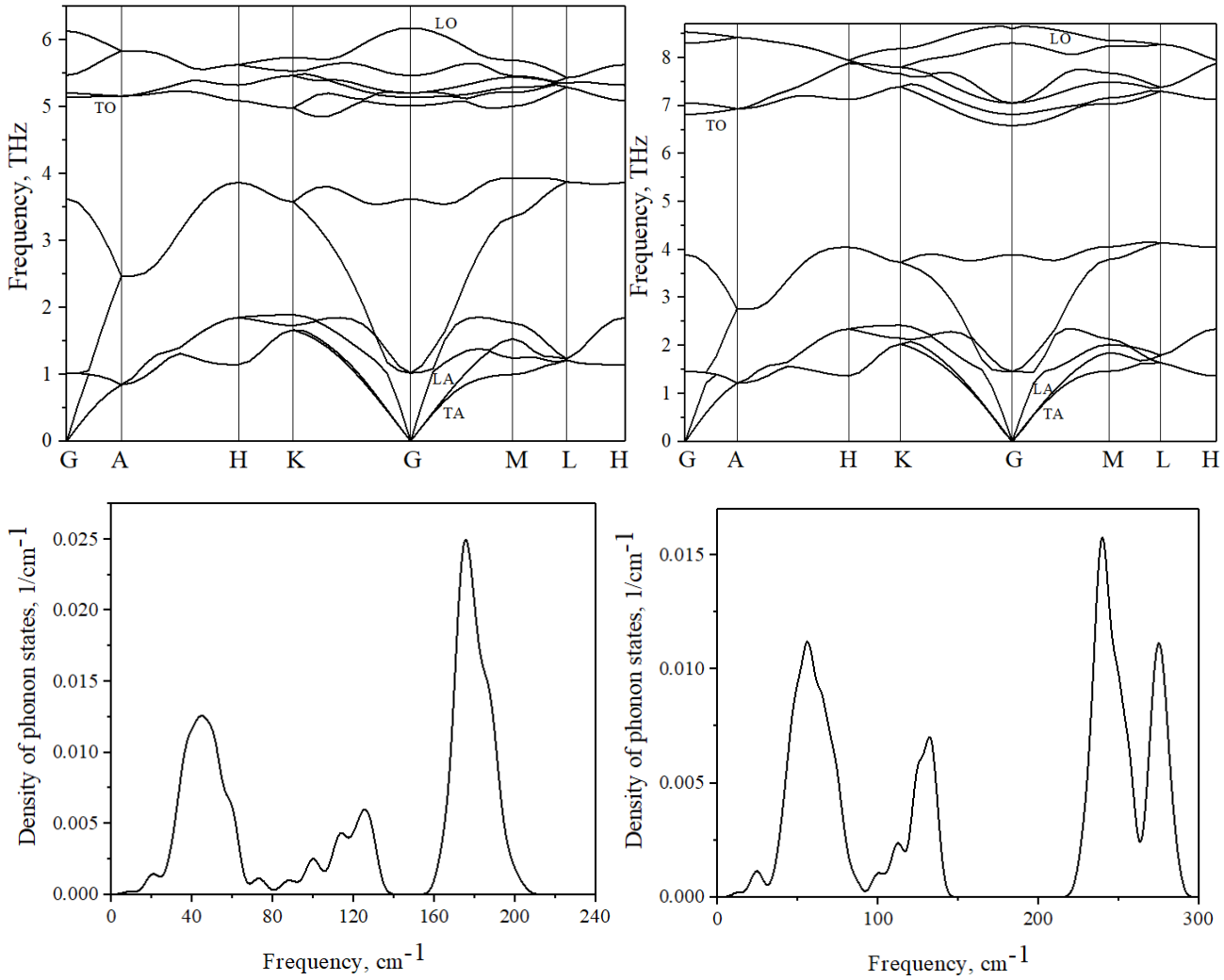

Fig. 3. The phonon dispersion ω_p curves and total phonon density of states of CdSe (a, c) and CdS (b, d) crystals

Phonon frequencies calculated at the high-symmetry points are also listed in Table 2. The optical and acoustic regions haven't crossed for both samples and the separation between the optical and acoustic regions increases from CdSe to CdS. Along the symmetry direction G→K (G→M), the TO branch is gradually increasing amount of upward dispersion as we move across CdSe–CdS, but LO branch is decreasing CdS–CdSe. The mass ratio of the basis atoms are 0.29 and 0.70 for CdS and CdSe, respectively. This mean that relative frequencies of the LO and TO modes are more strongly influenced by the mass ratio between the cation and anion as observed in Ref. [14, 15].

Table 2. The phonon frequencies (in THz) at the high-symmetry points G and L for CdS and CdSe, in hexagonal structure ($P6_3mc$) and the experimental finding

Sample	TO	LO	TA	LA	TO	LO
	G point in BZ		L point in BZ			
CdSe	5.02	6.17	1.21	1.23	5.29	5.44
CdS	6.59	8.54	1.64	1.79	7.30	8.28
CdSe[15]	5.93	6.53	1.27	4.18	6.13	6.12
CdS[15]	7.87	9.44	0.36	4.43	8.18	9.31

Fig. 4 shows theoretically calculated Raman spectra (RS) spectra of CdSe and CdS crystals at different temperatures between 0.1 and 1000 K. Series of peaks corresponding to vibrational modes of crystal structural elements were observed in the frequency range 0–240 cm^{-1}. RS are shows three peaks localization near 34, 168 and 172 cm^{-1} for CdSe and near 220, 227 and 235 cm^{-1} for CdS. All observed peaks were increases with increasing temperature (see Fig. 5).

Temperature dependence of Raman active bands shows parabolic behavior and don't shifted position with increasing temperature (see legend on Fig. 5). The calculated RS spectra agreed well with the experimental ones although peaks were slightly shifted. This could be due to specifics of DFT theory.

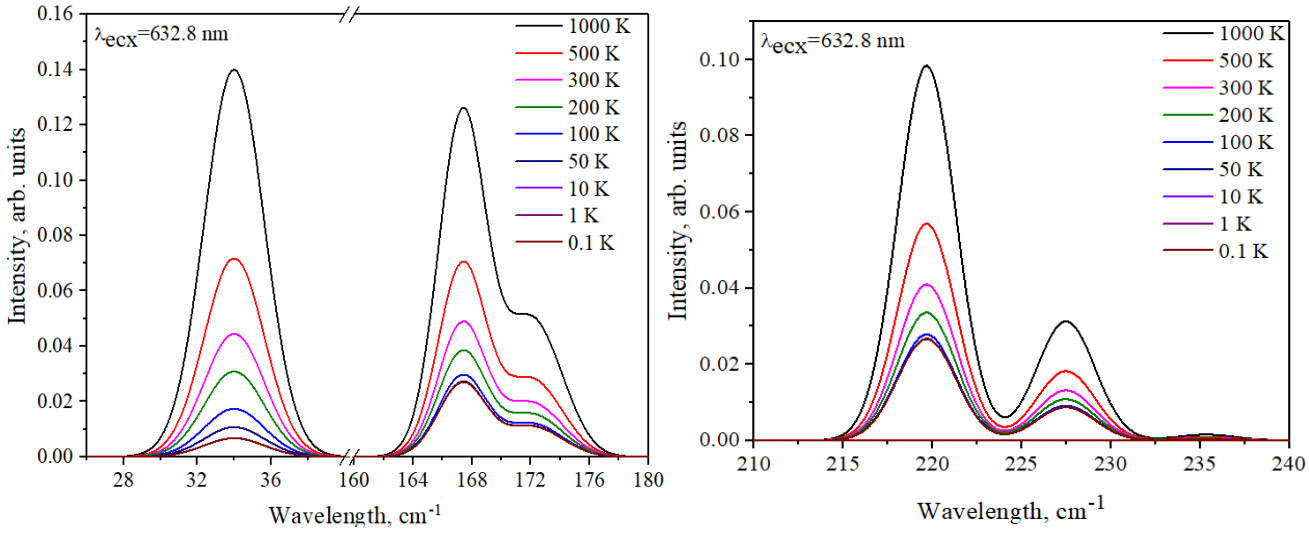

Fig. 4. RS of CdSe (a) and CdS (b) crystals at different temperatures (color online)

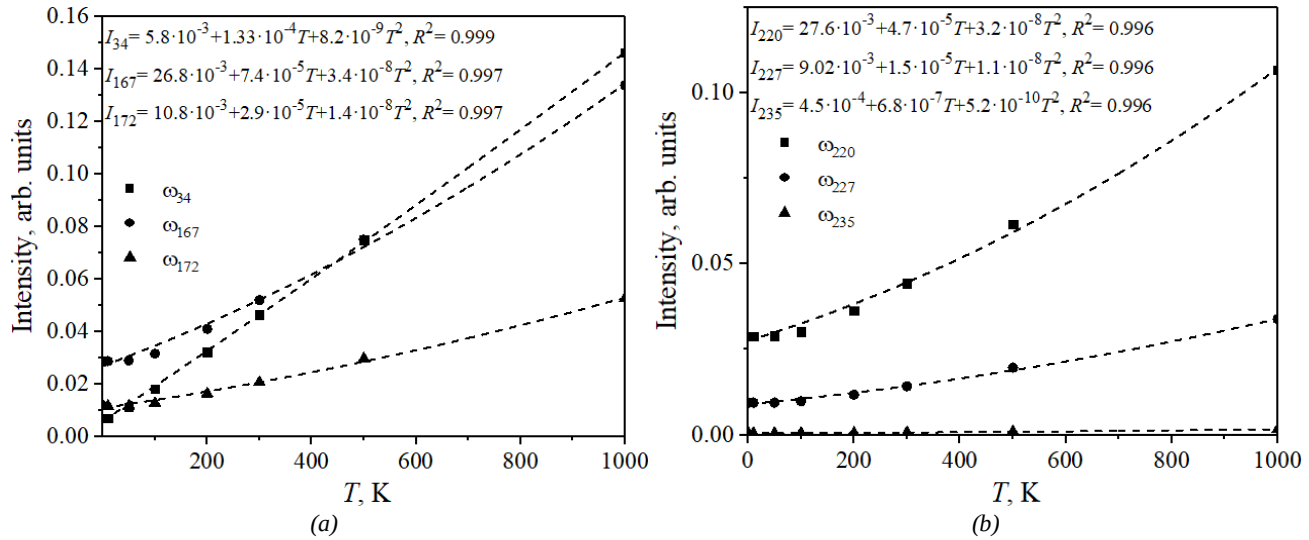

Fig. 5. Temperature dependence of intensity of the bands at RS for CdSe (a) and CdS (b) crystals. Legend: dashed line – functions of approximation, R^2 – determination coefficient; index at the marks frequency and intensity are corresponding to the value of peaks in RS

The theoretical calculations found that Cd–Se symmetric stretching modes contributed most to vibration in RS at the frequency 34 cm^{-1} (at 227 cm^{-1} in the case of CdS). Modes 168 cm^{-1} was Cd–Se compression modes (at 220 cm^{-1} in the case of CdS). Smaller intensity band at 172 cm^{-1} was determined by like Cd–Se symmetric scissoring modes (at 235 cm^{-1} in the case of CdS) (see Fig. 6).

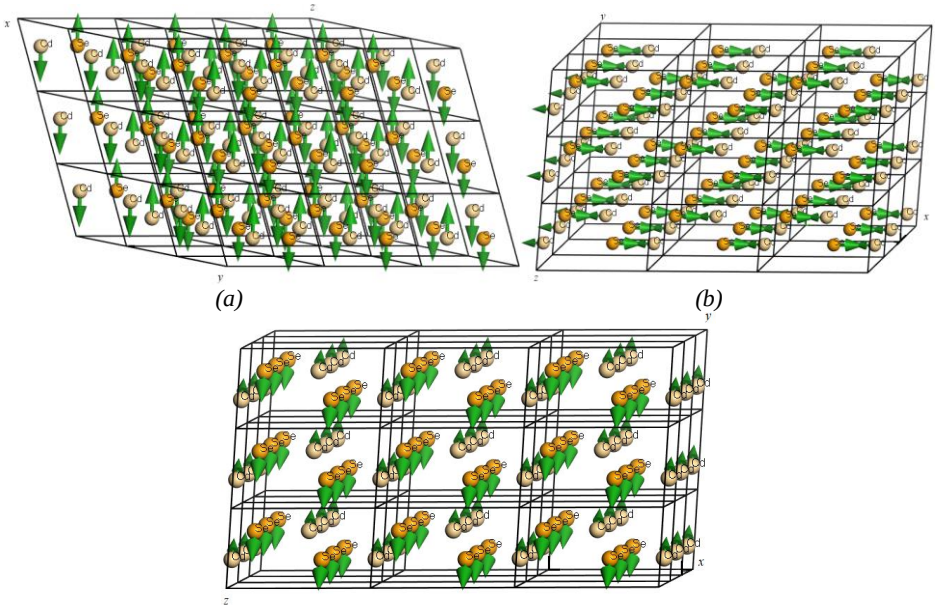

Fig. 6. Vibrations in the CdSe (a – 34 cm^{-1}, b – 168 cm^{-1}, c – 172 cm^{-1}) crystals (color online)

3.3. Optical properties

To study the optical properties, it is convenient to use a complex dielectric function $\varepsilon(\hbar\omega)$. The imaginary part of the dielectric function $\varepsilon(\hbar\omega)$ ($\varepsilon = \varepsilon_1 + i\varepsilon_2$) for CdSe and CdS crystals (Fig. 7) can be calculated using the relation (1). Then the real part of the $\varepsilon_1(\hbar\omega)$ function can be obtained from the Kramers–Kronig relation (2).

$$\varepsilon_2 = \frac{2e^2\pi}{V\varepsilon_0}\sum_{K,v,c}\left|\left\langle\psi_K^c\left|\hat{u}\cdot r\right|\psi_K^v\right\rangle\right|^2\delta\left(E_K^c - E_K^v - \hbar\omega\right) \quad (1)$$

$$\varepsilon_1 - 1 = \frac{2}{\pi}\int_0^\infty \frac{t\varepsilon_2(t)dt}{t^2 - (\hbar\omega)^2} \quad (2)$$

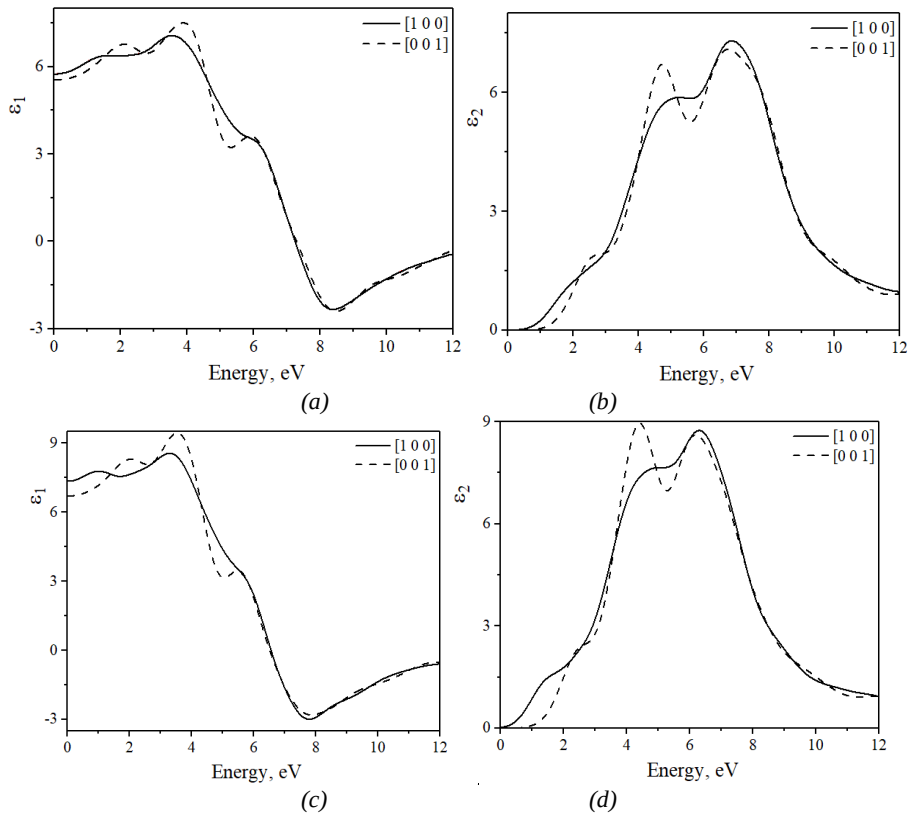

Fig. 7. Real (a, c) and imaginary (b, d) components of dielectric function ε calculated for CdS and CdSe crystals, respectively. (In legend: crystallographic directions of calculation)

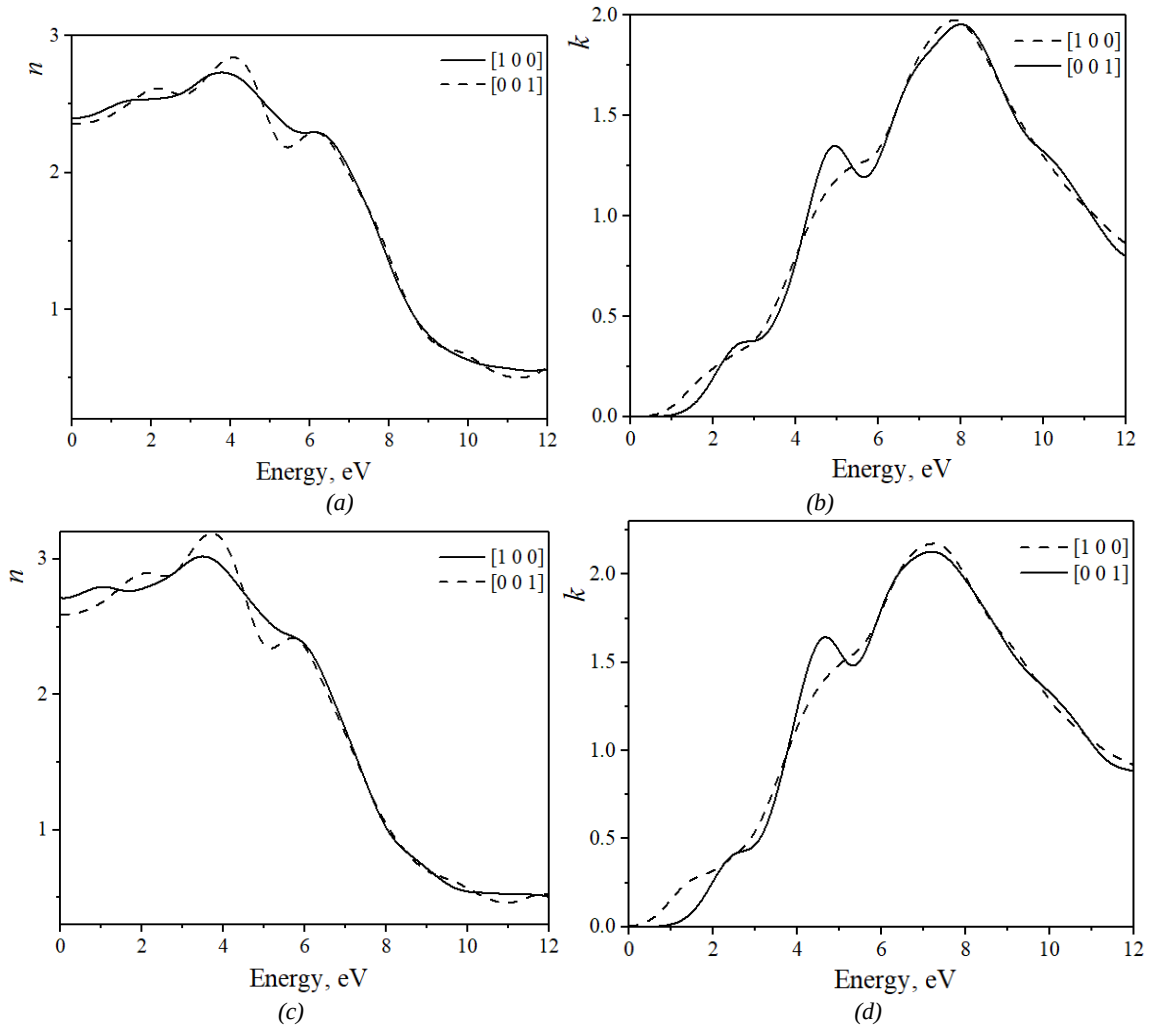

Fig. 8. Theoretically calculated spectra of refractive index (a, c) and extinction coefficient (b, d) for CdS and CdSe crystals, respectively (In legend: crystallographic directions of calculation)

As seen from the curve of the imaginary part of the dielectric function, the first critical point of the dielectric function in the form of fundamental absorption edge arises at an energy level of about 1.5 eV for CdS and about 0.7 eV for CdSe. With increasing energy, a typical rapid increase in the $\varepsilon_2(\hbar\omega)$ value is observed [3, 4]. We can observe a significant anisotropy of the dielectric function that varies with the optical polarization (see Fig. 7).

Using the calculated spectra for the real (Eq. (2)) and imaginary (Eq. (1)) parts of the dielectric function, one can obtain the following spectral dependences of the refractive index (n) and extinction coefficient (k):

$$n = \sqrt{\frac{(\varepsilon_1^2 + \varepsilon_2^2)^{1/2} + \varepsilon_1}{2}}, \quad k = \sqrt{\frac{(\varepsilon_1^2 + \varepsilon_2^2)^{1/2} - \varepsilon_1}{2}} \qquad (3)$$

The theoretical dependence of the refractive index for CdSe and CdS in the visible region of the spectrum is shown in Fig. 7. It is seen that the refractive index values satisfy the inequalities $n_{x,y} > n_z$ in the range of energies below 2 eV. The relative arrangement takes the form of $n_z > n_x$, in the range between 2 and 5 eV, and an inverse relationship is observed in the range of 6–12 eV. Such a deviation in the dynamics of the refractive index as a function of optical polarization is important for practical applications.

The refractive indices obtained theoretically are less than the experimental ones, which can be caused by the negative contribution of infrared absorption in the crystal, which has not been taken into account in the calculations (deviations ~ 20%). An analysis of the extinction coefficient (Fig. 8) confirms the anisotropy of the optical functions in low-energy region. This is manifested as a shift of the spectrum towards high energies ($k_{x,y} < k_z$). Such a behavior can be determined by the corresponding structural peculiarities ($a = b \neq c$) [4].

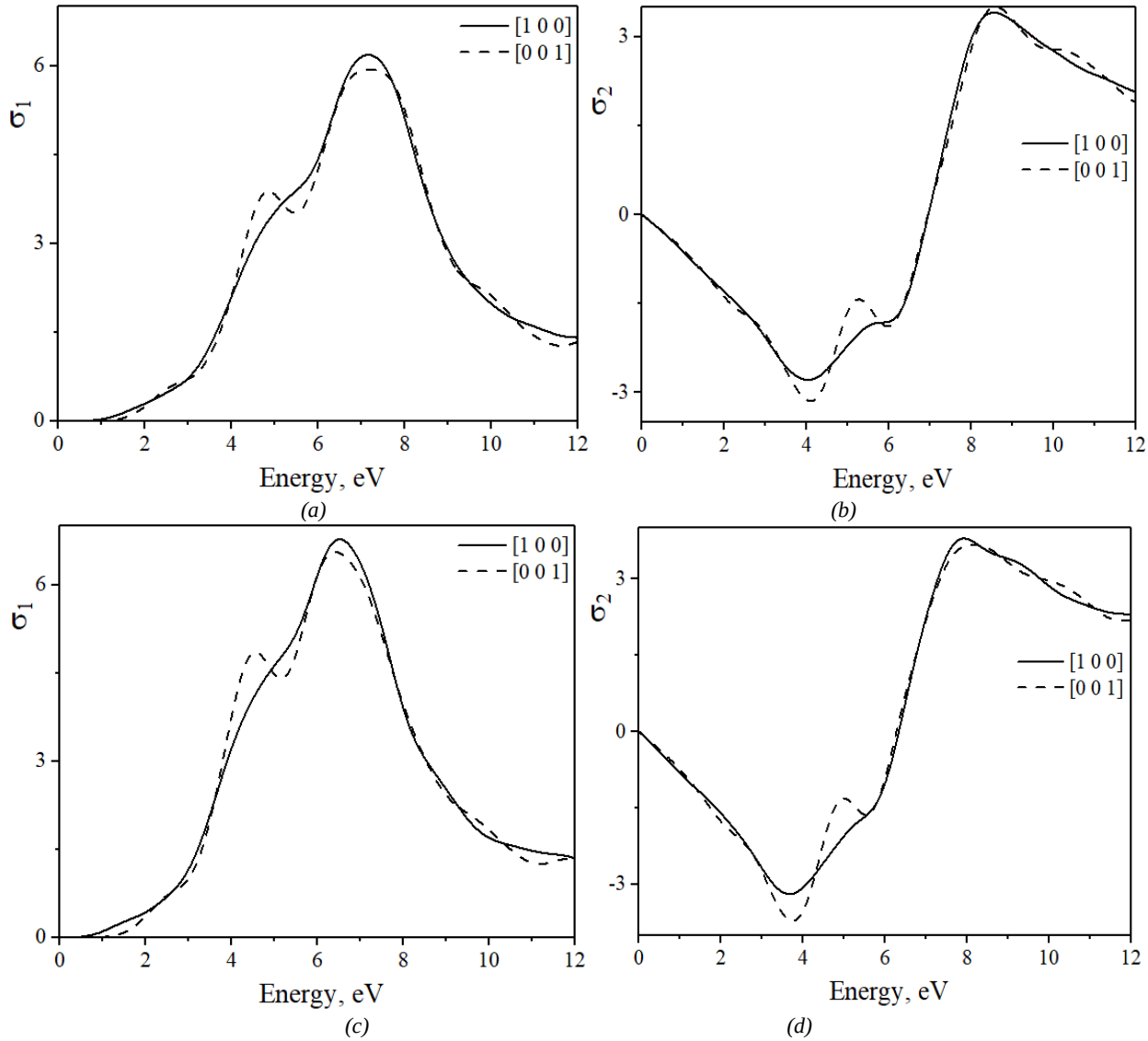

Fig. 9. Real (a, c) and imaginary (b, d) components of conductivity σ for CdS and CdSe crystals, respectively. (In legend: crystallographic directions of calculation)

Using the calculated spectra of the real and imaginary parts of the dielectric function (see Fig. 7), the spectral dependences of the optical conductivity (σ, see Fig. 9) can be obtained:

$$\sigma = \sigma_1 + i\sigma_2 = -i\frac{\omega}{4\pi}(\varepsilon - 1) \qquad (4)$$

3.4. Thermodynamics properties

The estimated temperature dependence features of free energy (F) and enthalpy (E) are presented in Fig. 10. As shows in Fig. 10, free energy (F) is decreases and tends to zero and negative values with increasing temperature, while the enthalpy (E) is increases. The calculated entropy (S) increases upon increasing temperature indicating that by raising temperature, it causes deeper oscillations of crystal planes.

Fig. 11 shows the constant-volume specific heat capacity for CdSe. As can be seen at high temperature, almost approaches the Petit-Dulong limit $3R$ (~24 J·mol^{-1}·K^{-1}) representing that at high temperature, all phonon modes are motivated by the thermal energy according to the observed behaviors of solids at high temperature [2].

The Debye temperature θ_D is one of the most important parameters that determine thermal properties of a material. The Debye temperature can be defined in terms of the mean acoustic velocity and gives explicit information about the lattice vibrations. This is the highest temperature that corresponds to the highest-frequency normal vibration ν_D, $\theta_D = h\nu_D / k_B$ (where $k_B = 1.380658 \cdot 10^{-23}$ J·K^{-1}). At relatively low temperatures, the vibrational excitations arise mainly due to acoustic oscillations. Notice that the value obtained for the Debye temperature (see Table 3) increases with increasing chalcogenides atomic charge and this behavior are correlated with other θ_D values.

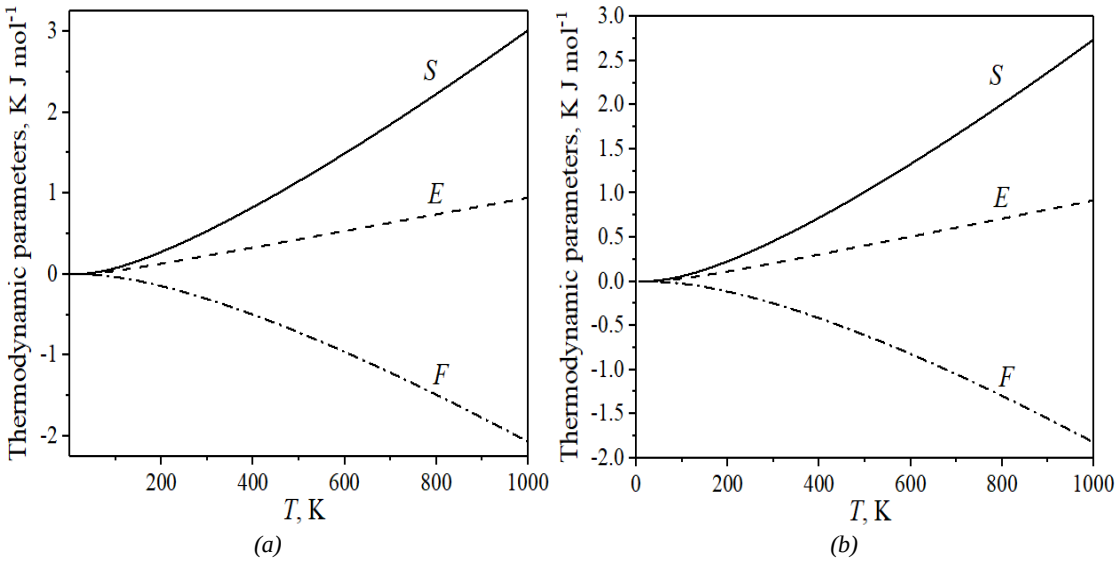

Fig. 10. Calculated temperature dependence (5–1000 K) of free energy (F) and enthalpy (E) and entropy (S) for CdSe (a) and CdS (b) crystals

Table 3. Debye temperature (in K) for CdS and CdSe crystals. T- temperature of for which measurements/calculations are performed

Material	Reference	θ_D	T, K
CdSe	This work	254.6	293
CdS		348	296
CdSe	[16]	317.6	298
CdSe	[17]	233.7	298
CdS	[18]	460	300

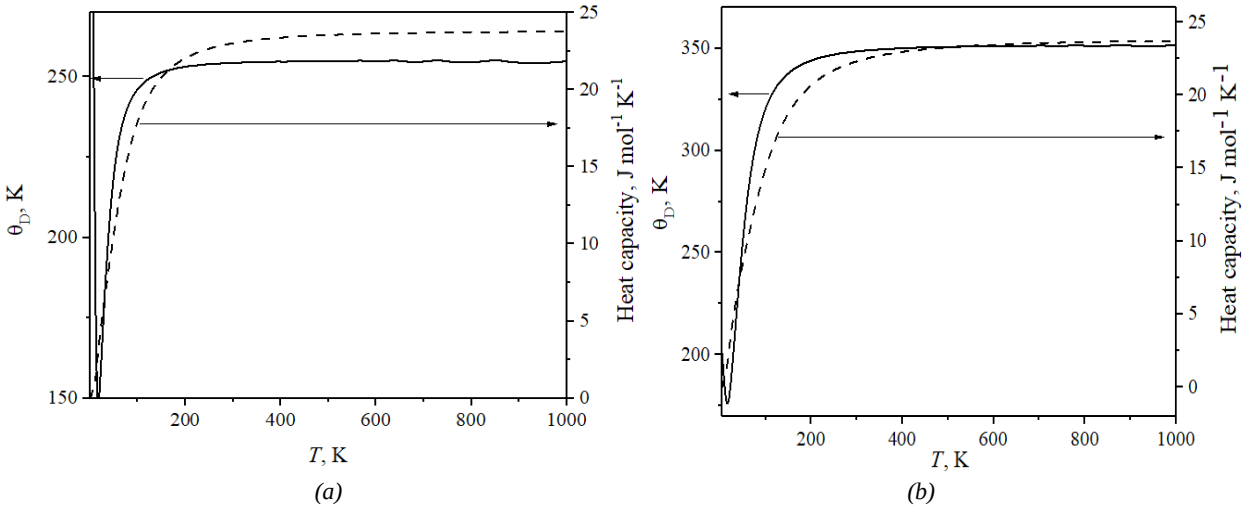

Fig. 11. Calculated temperature dependence (5–1000 K) of Debye temperature for CdSe (a) and CdS (b) crystals

4. Conclusion

Basing on the application of a number of modern theoretical approaches, in this work we elucidate a set of results that solve an important scientific and applied problem. The main results of the work reported in the present work can be summarized as follows:

First-principle theoretical studies of the electronic energy spectrum for the CdSe and CdS crystals have been carried out using the reliable techniques of density functional theory and known approximations. It has been established that the smallest bandgap is localized at the center of the BZ (i.e., at the point G). Therefore, our substances should reveal direct optical transitions. We have good agreement of obtained theoretical value of bandgap with known experimental results (1.128 eV for CdSe and 1.449 eV for CdS).

The phonon spectrum and frequencies of atomic vibrations in CdSe and CdS crystals were calculated using DFT. On the frequencies of the LO and TO modes are more strongly influenced by the mass ratio between the cation and anion as before assuming in literature. It was found that RS spectra calculated *ab initio* agreed rather well with the experimental data. Three peaks of RS were observed in both crystals which increase with increasing temperature. Temperature dependence of Raman active bands shows parabolic behavior and don't shifted position with increasing temperature.

To study the optical properties was use a complex dielectric function ε(ħω). Using Kramers–Kronig relation was calculation reflective index, extinction coefficient, real and imaginary part of dielectric function and optical conductivity.

Free energy is decreases and tends to zero and negative values with increasing temperature, while the enthalpy and entropy is increases, it causes deeper oscillations of crystal planes. At high temperature, all phonon modes are motivated by the thermal energy according to the observed behaviors of solids at high temperature. The value obtained for the Debye temperature correlates well with the other θ_D values.

Hence, the analysis of the fundamental physical properties of CdSe and CdS crystals which has been carried out in this work, makes it possible to proceed in the future to large-scale researches (2D and/or 0D structures based on these materials) aimed at producing the devices, which are based on these semiconductor compounds.

Acknowledgments

This work was supported by the Project of Young Scientists 0121U108649 of the Ministry of Education and Science of Ukraine.

References

[1] E. Deligoz, K. Colakoglu, Y. Ciftci, Physica B **373**(1), 124 (2006).
[2] F. B. Baghsiyahi, A. Akhtar, M. Yeganeh, International Journal of Modern Physics B **32**, 1850207 (2018).
[3] R. Yu. Petrus, H. A. Ilchuk, A. I. Kashuba, I. V. Semkiv, E. O. Zmiiovska, Optics and Spectroscopy **126**(3), 220 (2019).
[4] G. A. Ilchuk, R. Yu. Petrus, A. I. Kashuba, I. V. Semkiv, E. O. Zmiiovska, Optics and Spectroscopy **128**(1), 49 (2020).
[5] D. Vanderbilt, Phys. Rev. B **41**(11), 7892 (1990).
[6] J. P. Perdew, K. Burke, M. Ernzerhof, Phys. Rev. Lett. **78**(7), 1396 (1997).
[7] H. J. Monkhorst, J. D. Pack, Phys. Rev. B **13**(12), 5188 (1976).
[8] W. Shan, W. Walukiewicz, J. W. Ager, K. M. Yu, J. Wu, E. E. Haller, Applied Physics Letters **84**(1), 67 (2004).
[9] K. J. Hong, T. S. Jeong, C. J. Yoon, Y. J. Shin, Journal of Crystal Growth **218**, 19 (2000).
[10] H. Ilchuk, R. Petrus, A. Kashuba, I. Semkiv, E. Zmiiovska, Molecular Crystals and Liquid Crystals **699**(1), 1 (2020).
[11] W. Kohn, L. J. Sham, Phys. Rev. A **140**(4), 1133 (1965).
[12] P. A. Shchepanskyi, O. S. Kushnir, V. Yo. Stadnyk, A. O. Fedorchuk, M. Ya. Rudysh, R. S. Brezvin, P. Yu. Demchenko, A. S. Krymus, Ukr. J. Phys. Opt. **18**(4), 187 (2017).
[13] M. Ya. Rudys, P. A. Shchepanskyi, A. O. Fedorchuk, M. G. Brik, C.-G. Ma, G. L. Myronchuk, M. Piasecki, Journal of Alloys and Compounds **826**(15), 154232 (2020).
[14] G. P. Srivastava, H. M. Tutuncu, N. Gunhan, Phys. Rev. B **70**(8), 85206 (2004).
[15] E. Deligoz, K. Colakoglu, Y. Ciftci, Physica B **373**, 124 (2006).
[16] D. M. Freik, T. O. Parashchuk, B. P. Volochanska, Physics and Chemistry of Solid State **15**(2), 282 (2014).
[17] J. J. Tan, Y. Cheng, W.-J. Zhu, Q.-Q. Gou, Commun. Theor. Phys. **50**(1), 220 (2008).
[18] X. X. Yang, Z. F. Zhou, Y. Wang, R. Jiang, W. T. Zheng, Chang Q. Sun, Journal of Applied Physics **112**(8), 083508 (2012).

*Corresponding author: andrii.i.kashuba@lpnu.ua